

3-Dimensional Patient-Derived Lung Cancer Assays Reveal Resistance to Standards-of-Care Promoted by Stromal Cells but Sensitivity to Histone Deacetylase Inhibitors

David Onion^{1,2}, Richard H. Argent¹, Alexander M. Reece-Smith¹, Madeleine L. Craze¹, Robert G. Pineda¹, Philip A. Clarke¹, Hari L. Ratan³, Simon L. Parsons⁴, Dileep N. Lobo⁵, John P. Duffy⁶, John C. Atherton⁵, Andrew J. McKenzie⁷, Rajendra Kumari⁷, Peter King⁸, Brett M. Hall⁸, and Anna M. Grabowska¹

Abstract

There is a growing recognition that current preclinical models do not reflect the tumor microenvironment in cellular, biological, and biophysical content and this may have a profound effect on drug efficacy testing, especially in the era of molecular-targeted agents. Here, we describe a method to directly embed low-passage patient tumor-derived tissue into basement membrane extract, ensuring a low proportion of cell death to anoikis and growth complementation by coculture with patient-derived cancer-associated fibroblasts (CAF). A range of solid tumors proved amenable to growth and pharmacologic testing in this 3D assay. A study of 30 early-stage non-small cell lung cancer (NSCLC) specimens

revealed high levels of *de novo* resistance to a large range of standard-of-care agents, while histone deacetylase (HDAC) inhibitors and their combination with antineoplastic drugs displayed high levels of efficacy. Increased resistance was seen in the presence of patient-derived CAFs for many agents, highlighting the utility of the assay for tumor microenvironment-educated drug testing. Standard-of-care agents showed similar responses in the 3D *ex vivo* and patient-matched *in vivo* models validating the 3D-Tumor Growth Assay (3D-TGA) as a high-throughput screen for close-to-patient tumors using significantly reduced animal numbers. *Mol Cancer Ther*; 15(4): 753–63. ©2016 AACR.

Introduction

Currently, >90% of antineoplastic therapeutic agents that enter human clinical trials fail to become registered for clinical use (1), indicating the disconnect between current preclinical tumor

models and disease reality (2–4). Cell lines, grown in 2D *in vitro* culture and *in vivo* as subcutaneous tumors, are the most widely used tumor paradigm in both academic and pharmaceutical research. Whist readily available and easy to use, these models have been shown to be poorly predictive of clinical efficacy (5). By definition such lines have been selected for their ability to survive on 2D plastic surfaces and are known to drift in phenotype (6). Xenografts of such lines typically form rapidly growing, undifferentiated tumors, lacking the architecture and biological phenotype of the tumors that they are meant to represent. Drug resistance gene signatures of cell lines from the NCI-60 tumor panel in 2D or xenograft culture bare no relation to freshly isolated human tumor, being more closely matched to each other than the 6 tumor indications they represented (7).

Xenografts directly established from human tumors have tissue architecture and phenotype more closely resembling that of pancreatic (8), NSCLC (9, 10), and colorectal (11) cancers. Expansion of patient-derived tumors *in vivo* can provide material at early passage for *ex vivo* assays, such as the clonogenic assay, which show promising correlation between drug response *ex vivo* and that seen in the patient (12) but is not amenable to high-throughput screening. The influence of paracrine factors produced by tumor-recruited stroma and immune infiltrate on disease progression has been demonstrated (13, 14), but preclinical models incorporating heterogeneous cell populations are only just beginning to emerge (15).

Recently, there has been a move towards 3D *in vitro* cancer models (16). Cells grown on 2D culture surfaces display

¹Ex Vivo Cancer Pharmacology Centre of Excellence, Cancer Biology, Division of Cancer and Stem Cells, School of Medicine, University of Nottingham, Nottingham, United Kingdom. ²University of Nottingham Flow Cytometry Facility, School of Life Sciences, University of Nottingham, Nottingham, United Kingdom. ³Department of Urology, Nottingham University NHS Trust, QMC, Nottingham, United Kingdom. ⁴Nottingham University NHS Trust, City Hospital Campus, Nottingham, United Kingdom. ⁵Nottingham Digestive Diseases National Institute of Health Research Biomedical Research Unit, University of Nottingham and Nottingham University Hospitals NHS Trust, Nottingham, United Kingdom. ⁶Department of Thoracic Surgery, Nottingham University NHS Trust, City Hospital Campus, Nottingham United Kingdom. ⁷Crown Bioscience UK Ltd, Hillcrest, Loughborough, United Kingdom. ⁸Janssen Research and Development, Spring House, Pennsylvania.

Note: Supplementary data for this article are available at Molecular Cancer Therapeutics Online (<http://mct.aacrjournals.org/>).

Current Address for B.M. Hall: Molecular Response, 11011 Torreyana Road, Suite 200, San Diego, California.

Corresponding Author: Anna M. Grabowska, University of Nottingham, Queen's Medical Centre, West Block, D Floor, Nottingham NG7 2UH, UK. Phone: 115-8231135; Fax: 115-8231137; E-mail: anna.grabowska@nottingham.ac.uk

doi: 10.1158/1535-7163.MCT-15-0598

©2016 American Association for Cancer Research.

abnormal cell–cell interactions (17), cell–matrix interactions (if present; ref. 18) and are prone to spatial artifacts such as apical–basal polarization of fibroblasts (19) or inappropriate polarity and differentiation of epithelial cells (20). The overwhelming adhesion signaling from 2D culture can swamp growth factor signaling pathways, giving rise to unrepresentative pharmacologic responses to growth factor receptor inhibitors (21) or apoptosis-inducing agents (22), including chemotherapies (23). Therefore, 3D culture systems with minimal cell–cell, cell–matrix perturbations incorporating close-to-patient cells such as those generated in patient-derived xenograft (PDX) lines are required. Transition of cells between solid tumor xenografts and *in vitro* models has historically been problematic: direct transfer into traditional 2D tissue culture has a high attrition rate or results in growth of a highly selected subpopulation of cells so there is a need for models which avoid anoikis (24) and capture tumor heterogeneity.

We sought to develop a 3D *ex vivo* assay that was consistently capable of growing tumor cells with minimal loss from low-passage PDX lines, such that they were rapidly amenable to pharmacologic assay. We strove to align the biochemical and biophysical properties of the assay to the patient tumor micro-environment (TME). This was achieved by development of the 3-Dimensional Tumor Growth Assay (3D-TGA; refs. 25, 26), which utilizes a low stiffness laminin-rich extracellular matrix (ECM; ref. 27) to embed tumor cells and admixing with stromal cells to provide the paracrine signaling present in the TME of solid tumors (13, 14). We describe the establishment and application of a novel preclinical model utilizing tumor-derived ECM and incorporating patient-derived tumor-associated stromal cells which allows profiling of humanized close-to-patient xenografts at early passage.

Materials and Methods

Specimens and establishment of PDXs

Fresh surgical material from tumor resections at Nottingham University Hospitals NHS Trust, were collected with informed patient consent and National Research Ethics Service (NRES) approval (NRES REC 10/H0405/6). Samples were used in accordance with NRES approval (NRES REC 08/H0403/37). Samples of tumor tissue were dissected, formalin-fixed and paraffin-embedded (FFPE) for immunohistochemistry. A small amount of finely minced tumor tissue was enzymatically disaggregated (as below for xenograft tissue) and plated into 6-well tissue culture plates in DMEM, 10% FBS, 2 mmol/L glucose (Sigma) to establish fibroblasts; fibroblasts were banked at early passage and used in the 3D assay at less than passage 5. The majority of the finely minced tumor was mixed with bone marrow–derived mesenchymal stem cells (MSC) (5×10^5 /mouse) (ScienCell) and resuspended in ice-cold Matrigel (200 μ L/mouse; BD Biosciences). Animal procedures were carried out under UK Home Office Licence (PPL 40/3559) by qualified persons holding UK Home Office Personal Licences in accordance with the 3R's framework for humane animal research. Tumor samples were grafted subcutaneously into sex-matched MF-1 nude or NOD/SCID mice (Harlan). Initial grafting is referred to as passage 0 (P0). Upon growth, tumors were surgically removed under anesthesia, minced, and passaged on into further donor mice (P1, with the addition of MSCs and Matrigel as above) or taken for banking and 3D-TGA assays.

Disaggregation of xenograft tumors

Finely minced tumor was disaggregated using type II collagenase (100 U/mL; Invitrogen) and dispase (2.4 U/mL; Invitrogen) in HBSS (Sigma) at 37°C under constant rotation. Cells were removed at 1 to 2 hourly intervals until the tumor was completely disaggregated. Cell number and viability were determined using trypan blue exclusion and analyzed by flow cytometry for expression of EpCam (Supplementary Fig. S1 and Supplementary Methods).

The 3D-TGA

Cells were resuspended in ice-cold Cultrex basement membrane extract (BME) (3 mg/mL; Trevigen) diluted in modified RPMI-1640 (Life Technologies; phenol red free with 6 mmol/L D-glucose and pH6.8) and plated at 2.5×10^4 tumor cells $\pm 8.33 \times 10^3$ patient-derived CAFs/MSCs (ScienCell; per well (100 μ L) into low-adherent, black-walled, clear-bottom, 96-well plates (BrandTech) prewarmed to 37°C. CAFs derived from patient LU6 were used in all assays for NSCLC specimens and MSCs for all other tumor types. Drugs were serially diluted in modified RPMI-1640 and 50 μ L added in triplicate wells of the TGA on day 3. For the 384-well plate 3D-TGAs, a quarter of the 96-well plate cell number and volumes and six replicate wells were used. Drugs used in combination were premixed and serially diluted together before adding to the assay. Drug exposure was for 96 hours before final endpoint readings. The AlamarBlue assay [Invitrogen; 10% (v/v), 37°C for 1 hour] was used to monitor cell growth daily, using a fluorescent plate Reader (Flex Station II, Molecular Devices). Drug sensitivity was calculated as a percentage of matched untreated control and IC₅₀ curves were determined using GraphPad Prism 5 (GraphPad Software Inc., nonlinear curve fit of $Y = 100 / (1 + 10^{((\text{LogIC}_{50-X}) * \text{HillSlope}))}$). Error bars represent one standard deviation. Drugs in combination were at constant ratios to make them amenable to synergy testing using the Chou–Talay method (28) and CalcuSyn Software (Biosoft).

Immunohistochemistry

Immunohistochemistry and hematoxylin and eosin (H&E) staining were performed on 5- μ m tissue sections of FFPE tissue using standard techniques and the manufacturer's recommendations for the following primary antibodies: anti-human E-Cadherin (DAKO Clone NCH-38) and anti-human Vimentin (DAKO, Clone V9).

In vivo efficacy testing

Established PDXs from donor mice were surgically removed under anesthesia and tissue minced to passage on into mice for efficacy evaluation (passage 4–10, with the addition of MSCs and Matrigel as above). Procedures were carried out under UK Home Office Licence (PPL 70/7317). When tumors reached 150 to 200 mm³, 6 to 10 mice each were randomized to treatment and control groups, and treatment was initiated as follows: carboplatin/paclitaxel 50/5 mg/kg i.p. weekly, 100 mg/kg pemetrexed i.p. weekly, erlotinib (25 or 50 mg/kg p.o. q.d.) or matched vehicle control. Tumor size was measured using calipers (length and width) three times weekly, and tumor volumes were calculated by the formula: volume = (length + [width]²)/2).

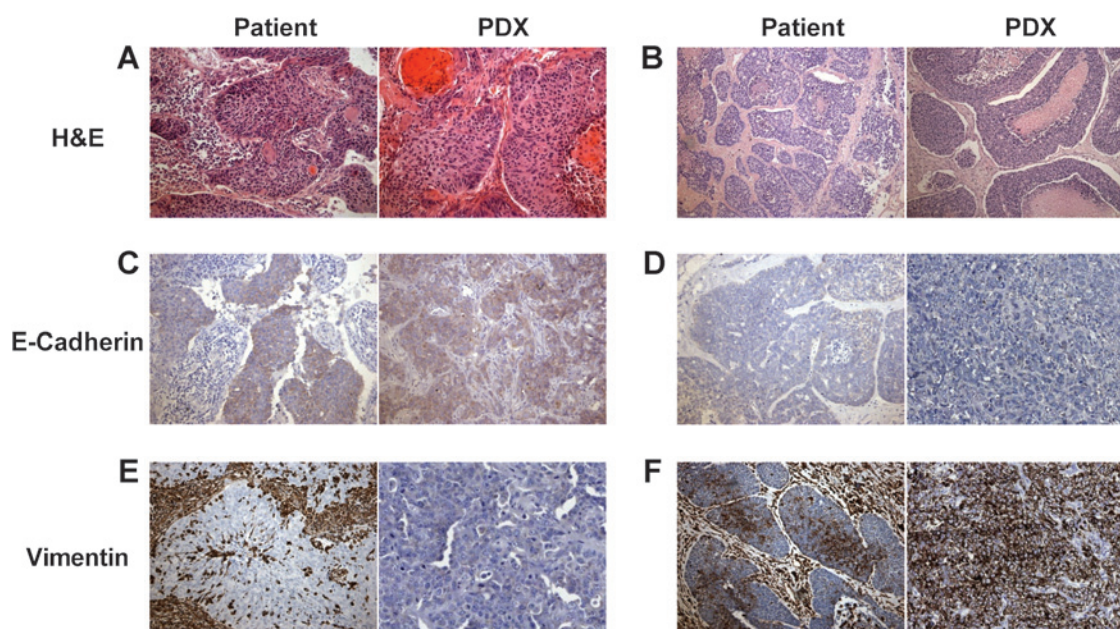


Figure 1. NSCLC PDX lines maintain architecture and EMT phenotype of original patient tumor. FFPE samples from matched patient and PDX samples were sectioned and stained with H&E to reveal architecture and by IHC for E-cadherin and vimentin for EMT phenotype. A, patient LU132 and P1 xenograft show destructive architecture. B, patient LU7 and P0 xenograft show an alveolar growth pattern. C and E, patient LU56 and P1 xenograft show epithelial phenotype. D and F, patient LU78 and P1 xenograft show mesenchymal phenotype.

Results

In vivo xenografts maintain growth pattern and transdifferentiation of original tumor

To determine how well PDXs of NSCLCs reflected their original primary tumor sample, matched tumor and sequential xenograft passages were profiled for growth pattern/architecture, and epithelial or mesenchymal phenotype. Of 36 successfully engrafted NSCLC tumors, 94% of the corresponding original patient tumor displayed a destructive (angiogenic) growth pattern (29, 30), with destruction of the normal lung parenchyma and infiltration with tumor-associated stroma (Fig. 1). This destructive pattern was maintained in all observed subsequent passages with murine stroma replacing the human counterpart over passage. The remaining two tumors displayed an alveolar growth pattern (nonangiogenic) with the tumor cell nest filling the alveolar spaces and areas of necrosis forming in central areas. In the corresponding xenografts, the gross morphology appeared to be maintained even in the absence of the alveolar septa. Tumor cell nests with small necrotic cores were organized by a surrounding web of stroma (Fig. 1). To determine whether there was phenotypic drift, epithelial and mesenchymal markers (E-cadherin and vimentin respectively) were quantified in 29 lines. Evidence of epithelial-to-mesenchymal transition (EMT) (absence of E-Cadherin or expression of vimentin in tumor cells) was seen in 38% (11/29) of patient tumors. Initial phenotype of tumor cells (epithelial or mesenchymal) was maintained in 79% (23/29) of cell lines, with one tumor showing some evidence of mesenchymal to epithelial transition (MET) and five showing signs of EMT (Fig. 1).

3D-TGA is a suitable microenvironment for PDXs from different tumor types and can be used to determine chemosensitivity in the presence and absence of stroma

Given the established PDX lines preserved the characteristics of the original patient tumor, we developed an *ex vivo* assay, utilizing tumor cells from the xenograft material, as both a surrogate model of the original tumor and a higher throughput alternative to PDX xenograft drug efficacy testing. To maximize the relevance of the TME-relevant *ex vivo* assay we adapted the 3D-TGA originally described by Sasser and colleagues (26) incorporating patient-derived tumor and stromal cells. Disaggregated xenografted tumors were cultured in the presence or absence of CAFs or MSCs (3:1 tumor: stroma ratio) in basement membrane extract. Tumor cells from NSCLCs ($n = 11$) were successfully grown in the 3D-TGA over a 7-day assay (Fig. 2 and Supplementary Figs. S2 and S3). Growth of tumor cells in 5 of 10 cases was enhanced in the presence of CAFs, including 1 example entirely dependent upon stromal support (LU42; see Supplementary Fig. S3). To monitor growth of stromal cells in cocultures independently of the tumor cells, CAFs constitutively expressing tdTomato were generated and growth monitored using tdTomato fluorescence. As expected in low stiffness matrix, stromal cells either alone or in coculture remained static or grew minimally through the assay, whereas tumor cells grew progressively (Supplementary Fig. S3).

Through the inclusion of serial dilutions of drug in the liquid overlay, the 3D-TGA was amenable for pharmacologic endpoint assay (Fig. 2). The applicability of this assay was further demonstrated in colorectal ($n = 9$), esophageal ($n = 1$), and pancreatic tumors ($n = 2$) and in colorectal lung metastases ($n = 5$; examples in Fig. 2A; growth curves in Supplementary Fig. S4), indicating that the 3D-TGA may be suitable for many solid tumor types.

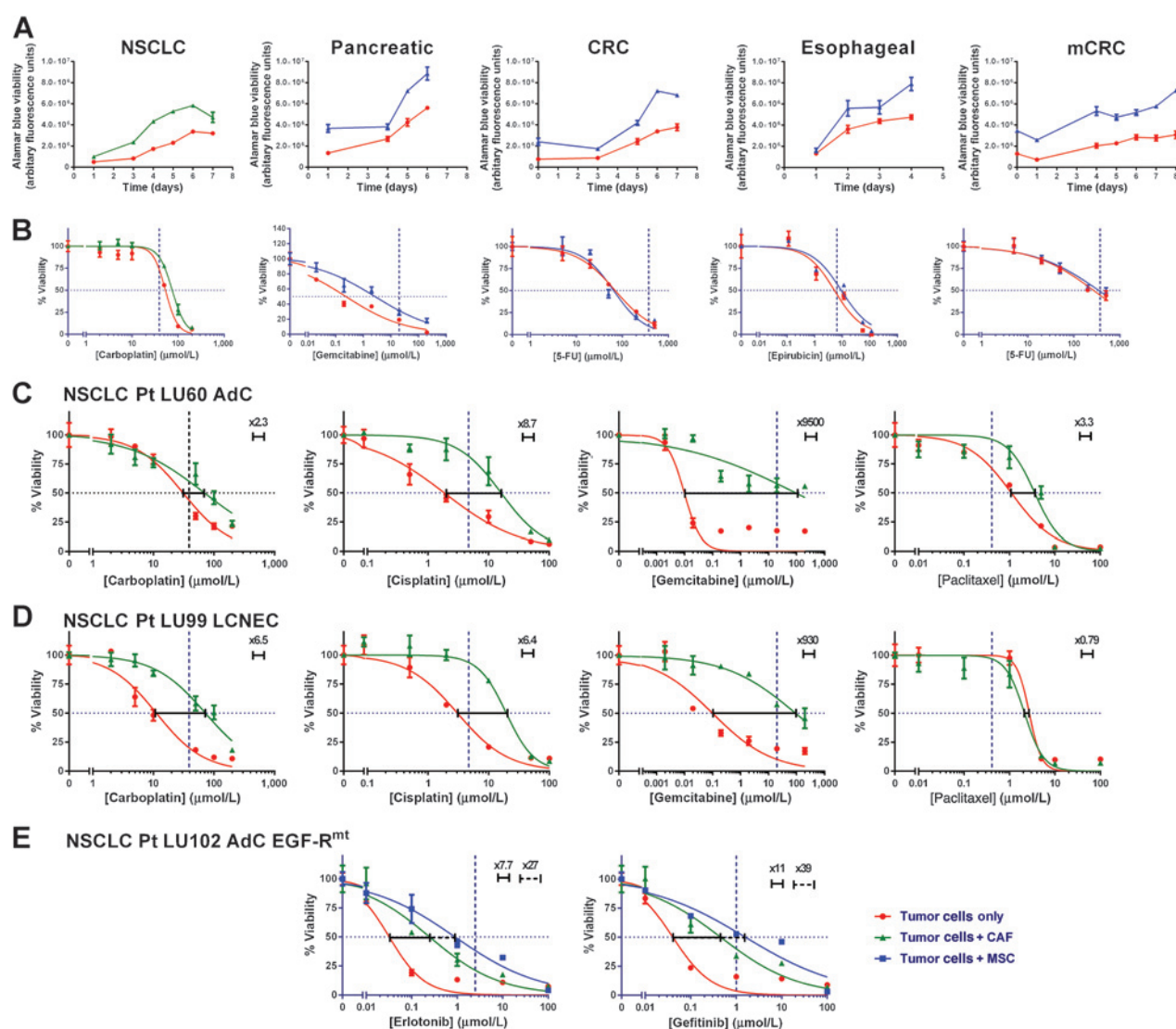


Figure 2. PDX tumor cell growth and drug sensitivity with supportive stroma in the 3D-TGA. A, representative growth of PDX-derived tumor cells in the 3D-TGA. Tumors were enzymatically disaggregated and single-cell suspensions entered into 3D-TGA with tumor cells only (red line) or in the presence of stromal cells (green line) at a ratio of 3 epithelial to 1 stromal cell. Growth was monitored by AlamarBlue fluorescent viability assay in triplicate wells; error bars, one standard deviation. B, drug sensitivity to SOC chemotherapeutics; drugs were overlaid on day 3 of assay and final day sensitivity assayed as a percentage of media-only control on day 7 by the AlamarBlue assay. Horizontal dotted lines, IC_{50} ; vertical dashed line, peak serum concentration of drug achieved in humans at typical doses; see Supplementary Table S1. C and D, examples of IC_{50} curves produced from PDX-derived tumor lines grown in the 3D-TGA, where the presence of patient-derived CAFs increased resistance to therapy. E, example of EGFR-mutant sensitivity to EGFR inhibitors and resistance induced by CAFs or MSCs. (m)CRC, (metastatic) colorectal carcinoma; AdC, adenocarcinoma; LCNEC, large-cell neuroendocrine carcinoma.

We observed low sensitivity to single standard-of-care (SOC) agents (carboplatin, cisplatin, gemcitabine, and paclitaxel) in NSCLC samples. There were some large changes in drug sensitivity to SOC agent in the presence of stromal cells (examples shown in Fig. 2C and D). LU60 (ADC) and LU99 (LCNEC) showed a modest increase in resistance (<10-fold) in the presence of CAFs in response to cisplatin, carboplatin or paclitaxel, but 9,500-fold (LU60) and 930-fold (LU99) decreases in sensitivity to gemcitabine when CAFs were present. This is an example that demonstrates models used in drug development that lack CAF interaction may fail to identify ineffective drugs.

A single patient (LU102) was found to harbor a point mutation in exon 21 of the tyrosine kinase domain (L858R) of EGFR, which results in oncogene-addiction and exquisite sensitivity to EGFR-TKIs such as erlotinib and gefitinib. In the 3D-TGA assay, LU102 showed nanomolar sensitivity to erlotinib and gefitinib. The presence of either CAFs or MSCs reduced the sensitivity in the EGFR-Rmutant patient when treated with erlotinib (CAF 7.7-fold, MSC 27-fold) and gefitinib (CAF 11.2-fold, MSC 39-fold; Fig. 2E). The CAFs and MSCs used are known to have high levels of *HGF* expression (Supplementary Fig. S5), which has been implicated in acquired stromal-induced resistance to EGFR inhibitors (31, 32).

3D-TGA modeling in early-stage NSCLC reveals broad levels of *de novo* drug resistance potentiated by the presence of stroma

To further investigate the sensitivity of PDX samples, 30 chemonaïve NSCLC patients were screened with a broad panel of single and combination SOC agents in the presence and absence of stromal support (Fig. 3A). To classify the relevance of individual drug-sensitivity results, IC₅₀ values were compared with maximum reported serum concentrations achievable in humans at typical human doses (Supplementary Table S1). Until the advent of targeted agents, the mainstay of chemotherapy for higher stage NSCLC has been platinum-based combinations. For both platinum agents (carboplatin and cisplatin) and other cytotoxic agents tested (docetaxel, gemcitabine, paclitaxel, pemetrexed, and vinorelbine), 50% or more patients were resistant when drugs were tested as single agents in the absence of stromal support and 70% or greater in the presence of stroma. For all drugs tested, the presence of stroma increased the number of patients showing drug resistance. Responses to combination of carboplatin/paclitaxel followed a similar pattern to those when tested as single agents, with low efficacy and increased resistance in the presence of stroma. In the absence of stroma, samples tested with combinations of cisplatin and either gemcitabine or vinorelbine showed the lowest levels of resistance (40% and 38%, respectively). The presence of stroma increased the number of samples classed as resistant for the gemcitabine/cisplatin combination; however, the combination of vinorelbine with cisplatin was almost unaffected by the presence of stroma. The vinorelbine/cisplatin combination was by far the most efficacious modality tested in the presence of stroma, with 50% of patients showing drug sensitivity. Figure 3B shows individual patient IC₅₀ values for cisplatin, vinorelbine, and their combination (data for all drugs in Supplementary Fig. S6), where it can be seen that the presence of patient-derived CAFs causes a statistically significant decrease in sensitivity to both single agents while no difference was observed when tested in combination.

Overall, the data for cytotoxic reagents reflects the very poor response rates to standard chemotherapies seen in the clinic where they are predominately used in higher stage patients and indicates an intrinsic disease-specific resistance to these therapies rather than one associated with late-stage disease or acquired resistance. The presence of CAFs caused a modest overall increase in resistance to SOC; however, there were noticeable individual examples where the presence of CAFs profoundly altered drug sensitivity (Fig. 2).

EGFR tyrosine kinase (TK)-targeted agents erlotinib and gefitinib were tested as single agents and only 1 of 30 patients showed response. Indeed, this was the only patient (LU102 discussed above) shown to have a mutated EGFR and displayed nanomolar sensitivity, >1,000-fold more sensitive than patients with the rest of the cohort (mean IC₅₀ for erlotinib treatment of EGFR^{WT} = 34 μmol/L and LU102 EGFR^{mt} = 0.03 nmol/L; Fig. 2).

HDAC inhibitors JNJ-26481585 and panobinostat efficiently kill multidrug-resistant NSCLC specimens

There is a clinical need for antineoplastic agents with greater efficacy in the NSCLC setting and given the cohort of patients studied here showed a high degree of *de novo* resistance to SOC agents, novel therapies were considered. HDAC inhibitors induce apoptosis, cell-cycle arrest, and terminal differentiation in a variety of human tumors and, while currently only clinically licensed for hematological malignancies, show promise in solid

tumors, including NSCLC (33). Three class I HDAC inhibitors—JNJ-26481585 (34, 35), panobinostat, and vorinostat—were tested in the panel of patient-derived NSCLC specimens. Samples were classified as sensitive, if the IC₅₀ was below the achievable serum concentrations in humans (1.5 μmol/L panobinostat, 1.81 μmol/L vorinostat: see Supplementary Table S1); as this information was unavailable for JNJ-26481585, 1 μmol/L was arbitrarily set as the cutoff. Patient samples showed a high level of sensitivity to both JNJ-26481585 (83%, 24/29) and panobinostat (80%, 16/20) with nanomolar IC₅₀s (Fig. 4). While the number of those classified as sensitive was the same in the presence or absence of patient-derived CAFs, for both JNJ-26481585 and panobinostat there was a significant increase in IC₅₀ values in samples tested in the presence of CAFs (Supplementary Fig. S7). Vorinostat was less efficacious, with only 33% (7/21) and 5% (1/21) of patient samples showing sensitivity in the absence or presence of CAFs, respectively. The clinical toxicity of high-dose HDAC inhibitors may limit their use as single agents; however, there is the potential that global epigenetic changes can resensitize resistant tumors to SOC agents. JNJ-26481585 was tested in combination with SOC agents cisplatin, gemcitabine, vinorelbine, or pemetrexed (adenocarcinomas only). As the majority of samples were sensitive to the JNJ-26481585 single agent, high sensitivities were seen to the combinations. Positive interactions between JNJ-26481585 and SOC agents (additive or synergistic) were seen for 57% of samples tested. Of note, two samples (LU91 and LU108), which showed low sensitivity to SOC agents and JNJ-26481585 as single agents, had favorable interaction with all three SOC agents tested (vinorelbine, cisplatin, and gemcitabine). However, in the case of LU91 and LU108 this increased sensitivity was not sufficient to bring IC₅₀ values into clinical relevant range (Fig. 4). There was one example of dramatic synergy between JNJ-26481585 and gemcitabine in patient LU126 where the addition of 5 nmol/L JNJ-26481585 to gemcitabine reduced the IC₅₀ by over 1,000-fold (Fig. 4B–D).

3D-TGA recapitulates *in vivo* PDX SOC sensitivities

Sensitivity to SOC agents was determined in PDX *in vivo* models, and data were compared with that generated from 3D-TGA line at early passage. PDX lines from 10 patients were passaged into MF-1 nude mice and treated with paclitaxel/carboplatin combination or pemetrexed. Responses were determined by measurement of mean tumor volume in comparison with vehicle control. The majority of PDX lines showed *de novo* resistance to SOC agents, with 10 of 10 showing no response to pemetrexed and only 3 of 10 showing response to carboplatin/paclitaxel combination. As shown in Fig. 5 these correlated with data from 3D-TGA in which all lines were resistant to pemetrexed whereas LU11, LU57, and LU78 showed some sensitivity to paclitaxel/carboplatin. Interestingly in the 3D-TGA it was clear that LU78 was sensitive to carboplatin as a single agent, whereas LU11 and LU57 only showed sensitivity to the combination. Additionally, LU102 demonstrated sensitivity to erlotinib *in vivo* (as it did in 3D-TGA), where a dramatic sensitivity was observed, with reduction and elimination of established tumors (Fig. 5D).

Discussion

Here, we describe a novel *ex vivo* 3D assay which uses close-to-patient material, derived from PDX models, with matched stromal support to determine drug sensitivity in a cohort of stage I to

A

LU	Histology	Carboplatin		Cisplatin		Docetaxol		Erlotinib		Gefitinib		Gemcitabine		Paclitaxel		Pemetrexed		Vinorelbine		Carbo/Pacdi		Gem/Cis		Vin/Cis		Pem/Cis			
		-	+	-	+	-	+	-	+	-	+	-	+	-	+	-	+	-	+	-	+	-	+	-	+	-	+	-	+
		CAF	CAF	CAF	CAF	CAF	CAF	CAF	CAF	CAF	CAF	CAF	CAF	CAF	CAF	CAF	CAF	CAF	CAF	CAF	CAF	CAF	CAF	CAF	CAF	CAF	CAF	CAF	CAF
2	NSCLC-SCC	Red	Red	Red	Red	Red	Red	Red	Red	Red	Red	Red	Red	Red	Red	Red	Red	Red	Red	Red	Red	Red	Red	Red	Red	Red	Red		
8	NSCLC-SCC	Red	Red	Red	Red	Green	Green	Red	Red	Red	Red	Red	Red	Red	Red	Red	Red	Red	Red	Red	Red	Red	Red	Red	Red	Red	Red		
11	NSCLC-SCC	Red	Red	Red	Red	Red	Red	Red	Red	Red	Red	Red	Red	Red	Red	Red	Red	Red	Red	Red	Red	Red	Red	Red	Red	Red	Red		
12	NSCLC-SCC	Red	Red	Red	Red	Red	Red	Red	Red	Red	Red	Red	Red	Red	Red	Red	Red	Red	Red	Red	Red	Red	Red	Red	Red	Red	Red		
48	NSCLC-SCC	Red	Red	Red	Red	Red	Red	Red	Red	Red	Red	Red	Red	Red	Red	Red	Red	Red	Red	Red	Red	Red	Red	Red	Red	Red	Red		
52	NSCLC-AdS	Red	Red	Red	Red	Red	Red	Red	Red	Red	Red	Red	Red	Red	Red	Red	Red	Red	Red	Red	Red	Red	Red	Red	Red	Red	Red		
55	NSCLC-SCC	Red	Red	Red	Red	Red	Red	Red	Red	Red	Red	Red	Red	Red	Red	Red	Red	Red	Red	Red	Red	Red	Red	Red	Red	Red	Red		
56	NSCLC-AdC	Red	Red	Red	Red	Red	Red	Red	Red	Red	Red	Red	Red	Red	Red	Red	Red	Red	Red	Red	Red	Red	Red	Red	Red	Red	Red		
57	NSCLC-SCC	Red	Red	Red	Red	Red	Red	Red	Red	Red	Red	Red	Red	Red	Red	Red	Red	Red	Red	Red	Red	Red	Red	Red	Red	Red	Red		
60	NSCLC-AdC	Red	Red	Red	Red	Red	Red	Red	Red	Red	Red	Red	Red	Red	Red	Red	Red	Red	Red	Red	Red	Red	Red	Red	Red	Red	Red		
73	NSCLC-SCC	Red	Red	Red	Red	Red	Red	Red	Red	Red	Red	Red	Red	Red	Red	Red	Red	Red	Red	Red	Red	Red	Red	Red	Red	Red	Red		
78	NSCLC-AdC	Red	Red	Red	Red	Red	Red	Red	Red	Red	Red	Red	Red	Red	Red	Red	Red	Red	Red	Red	Red	Red	Red	Red	Red	Red	Red		
91	NSCLC-SCC	Red	Red	Red	Red	Red	Red	Red	Red	Red	Red	Red	Red	Red	Red	Red	Red	Red	Red	Red	Red	Red	Red	Red	Red	Red	Red		
97	NSCLC-SCC	Red	Red	Red	Red	Red	Red	Red	Red	Red	Red	Red	Red	Red	Red	Red	Red	Red	Red	Red	Red	Red	Red	Red	Red	Red	Red		
102	NSCLC-AdC	Red	Red	Red	Red	Red	Red	Red	Red	Red	Red	Red	Red	Red	Red	Red	Red	Red	Red	Red	Red	Red	Red	Red	Red	Red	Red		
105	NSCLC-AdC	Red	Red	Red	Red	Red	Red	Red	Red	Red	Red	Red	Red	Red	Red	Red	Red	Red	Red	Red	Red	Red	Red	Red	Red	Red	Red		
108	NSCLC-AdC	Red	Red	Red	Red	Red	Red	Red	Red	Red	Red	Red	Red	Red	Red	Red	Red	Red	Red	Red	Red	Red	Red	Red	Red	Red	Red		
116	NSCLC-SCC	Red	Red	Red	Red	Red	Red	Red	Red	Red	Red	Red	Red	Red	Red	Red	Red	Red	Red	Red	Red	Red	Red	Red	Red	Red	Red		
126	NSCLC-AdC	Red	Red	Red	Red	Red	Red	Red	Red	Red	Red	Red	Red	Red	Red	Red	Red	Red	Red	Red	Red	Red	Red	Red	Red	Red	Red		
137	NSCLC-SCC	Red	Red	Red	Red	Red	Red	Red	Red	Red	Red	Red	Red	Red	Red	Red	Red	Red	Red	Red	Red	Red	Red	Red	Red	Red	Red		
165	NSCLC-SCC	Red	Red	Red	Red	Red	Red	Red	Red	Red	Red	Red	Red	Red	Red	Red	Red	Red	Red	Red	Red	Red	Red	Red	Red	Red	Red		
168	NSCLC-SCC	Red	Red	Red	Red	Red	Red	Red	Red	Red	Red	Red	Red	Red	Red	Red	Red	Red	Red	Red	Red	Red	Red	Red	Red	Red	Red		
182	NSCLC-SCC	Red	Red	Red	Red	Red	Red	Red	Red	Red	Red	Red	Red	Red	Red	Red	Red	Red	Red	Red	Red	Red	Red	Red	Red	Red	Red		
192	NSCLC-SCC	Red	Red	Red	Red	Red	Red	Red	Red	Red	Red	Red	Red	Red	Red	Red	Red	Red	Red	Red	Red	Red	Red	Red	Red	Red	Red		
204	NSCLC-SCC	Red	Red	Red	Red	Red	Red	Red	Red	Red	Red	Red	Red	Red	Red	Red	Red	Red	Red	Red	Red	Red	Red	Red	Red	Red	Red		
215	NSCLC-SCC	Red	Red	Red	Red	Red	Red	Red	Red	Red	Red	Red	Red	Red	Red	Red	Red	Red	Red	Red	Red	Red	Red	Red	Red	Red	Red		
221	NSCLC-UN	Red	Red	Red	Red	Red	Red	Red	Red	Red	Red	Red	Red	Red	Red	Red	Red	Red	Red	Red	Red	Red	Red	Red	Red	Red	Red		
238	NSCLC-SCC	Red	Red	Red	Red	Red	Red	Red	Red	Red	Red	Red	Red	Red	Red	Red	Red	Red	Red	Red	Red	Red	Red	Red	Red	Red	Red		
259	NSCLC-SCC	Red	Red	Red	Red	Red	Red	Red	Red	Red	Red	Red	Red	Red	Red	Red	Red	Red	Red	Red	Red	Red	Red	Red	Red	Red	Red		
282	NSCLC-SCC	Red	Red	Red	Red	Red	Red	Red	Red	Red	Red	Red	Red	Red	Red	Red	Red	Red	Red	Red	Red	Red	Red	Red	Red	Red	Red		
%	Sensitive	43.33	16.67	26.67	3.33	33.33	23.33	3.33	3.45	3.45	3.45	33.33	3.33	10.00	10.00	0.00	0.00	20.00	3.33	45.00	16.67	60.00	30.00	53.85	50.00	33.33	16.67		
%	Borderline	6.67	13.33	10.00	0.00	3.33	3.33	3.33	0.00	0.00	0.00	3.33	0.00	16.67	3.33	3.33	0.00	6.67	3.33	5.00	3.33	0.00	3.33	7.69	15.38	0.00	0.00		
%	Resistant	50.00	70.00	63.33	96.67	63.33	73.33	93.33	96.55	96.55	96.55	63.33	96.67	73.33	86.67	96.67	100.00	73.33	93.33	50.00	80.00	40.00	66.67	38.46	34.62	66.67	83.33		

B

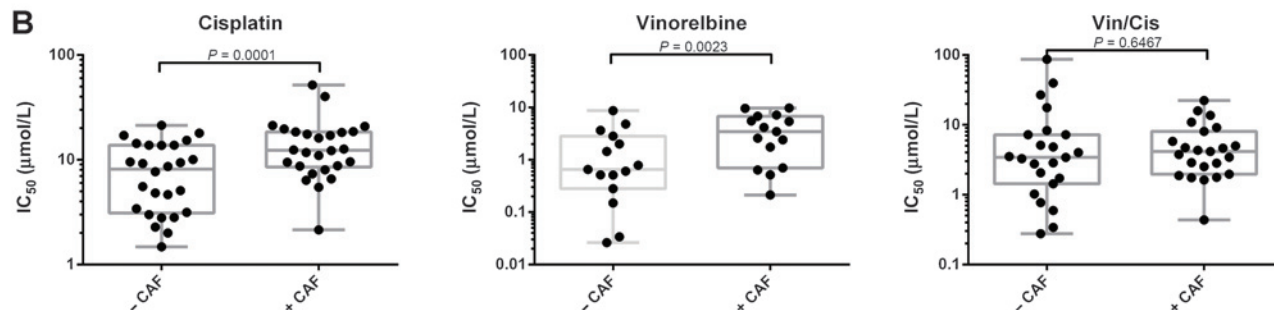


Figure 3.

Drug sensitivity of NSCLC patient lines to SOC agents in 3D-TGA. PDX-derived tumor cells ($n = 30$) were grown in the 3D-TGA in the presence or absence of patient-derived CAFs and serial drug dilution was applied on day 3 as single agents or combinations at fixed ratio. A, endpoint cell viability was measured at day 7 by AlamarBlue assay; IC₅₀ curves were generated using GraphPad Prism Software; and samples were classified as sensitive (green), borderline (amber), and resistant (red) in comparison with achievable serum concentrations in humans (Supplementary Table S1): sensitive (<90%), borderline (90%–110%), resistant (>110%). White boxes not done. B, sensitivity of patient cells to cisplatin and vinorelbine but not their combination is reduced in the presence of CAFs. Paired IC₅₀ values for individual patients in the presence and absence of CAFs are shown, with mean and range shown by box and whiskers. Significance of difference is shown as P value calculated by ratio paired t test. AdC, adenocarcinoma; AdS, adenocarcinoma; SCC, squamous cell carcinoma; UN, unknown; carbo, carboplatin; paci, paclitaxel; gem, gemcitabine; cis, cisplatin; vin, vinorelbine; pem, pemetrexed.

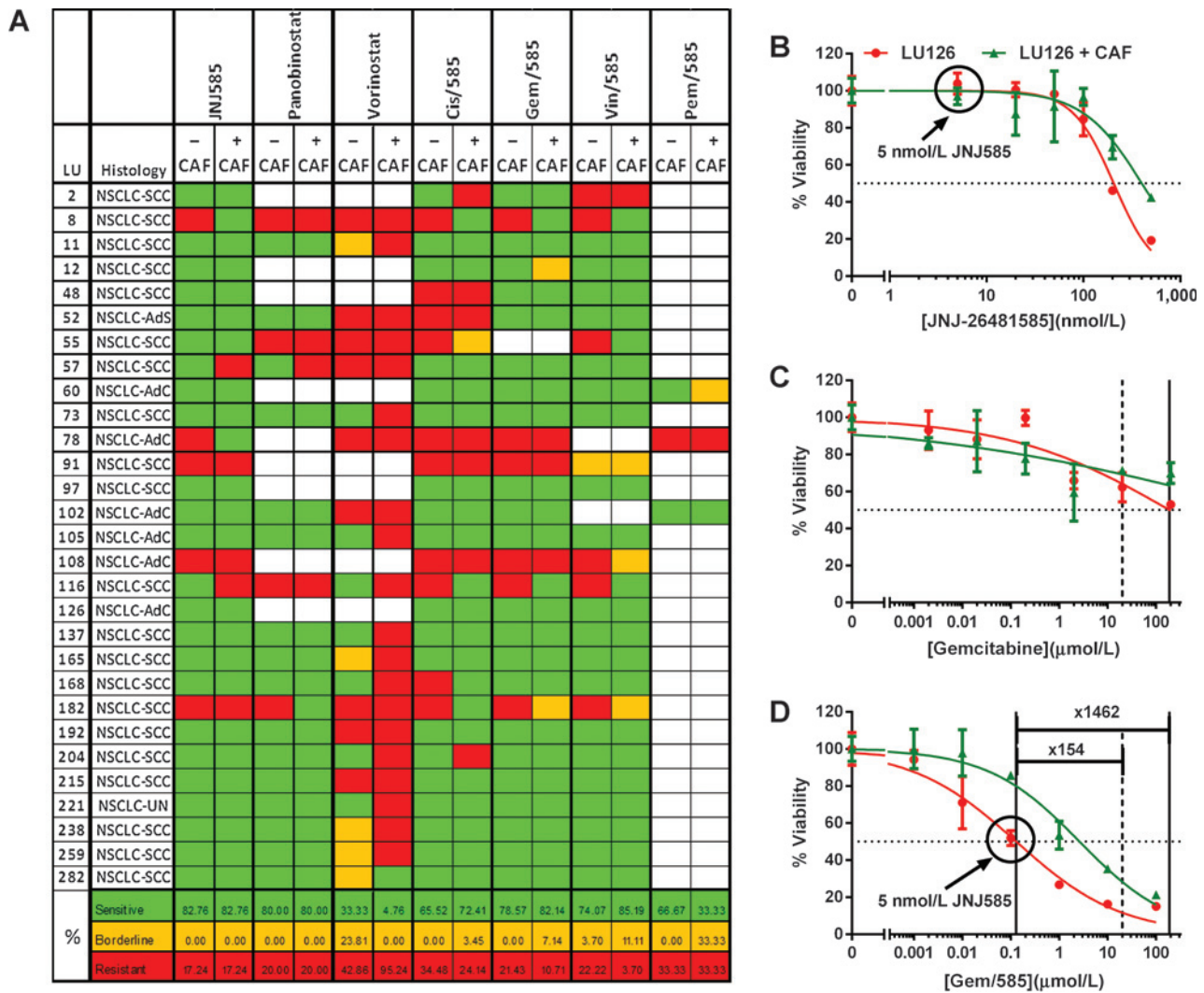


Figure 4. Drug sensitivity of NSCLC patient lines to HDAC inhibitors in 3D-TGA. PDX-derived tumor cells ($n = 29$) were grown in the 3D-TGA in the presence or absence of patient-derived CAFs, and serial drug dilution was applied on day 3 as single agents or combinations at fixed ratio. Endpoint cell viability was measured at day 7 by AlamarBlue assay, and IC_{50} curves were generated using GraphPad Prism Software. A, summary table with samples classified as sensitive (green), borderline (amber), and resistant (red) in comparison with achievable serum concentrations in humans (1.5 $\mu\text{mol/L}$ panobinostat, 1.81 $\mu\text{mol/L}$ vorinostat) and for JNJ-26481585 (JNJ585) arbitrarily at 1 $\mu\text{mol/L}$: sensitive (<90%), borderline (90%–110%), resistant (>110%). White boxes, not done. B–D, example of synergy seen with LU126. B, JNJ26481585 single agent. C, gemcitabine single agent. D, gemcitabine/JNJ26481585 (10:1 molar ratio; scale gemcitabine). AdC, adenocarcinoma; AdS, adenosquamous; SCC, squamous cell carcinoma; UN, unknown; carbo, carboplatin; pacli, paclitaxel; gem, gemcitabine; cis, cisplatin; vin, vinorelbine; pem, pemetrexed; 585, JNJ-26481585.

III NSCLC patients undergoing surgery. Despite most of the patients being chemotherapy naïve, the majority showed high levels of intrinsic resistance to a panel of SOC agents and combinations, with many showing higher levels of resistance when tested in the presence of CAFs. HDAC inhibitors JNJ-26481585 and panobinostat showed promising results, including when tested in combination with current SOC agents, underlining their promise for solid tumor therapy. The 3D-TGA showed broader applicability across other tumor indications and, in a cohort of 10 patients, correlation between the 3D-TGA and standard *in vivo* xenograft sensitivity testing indicated both its relevance and potential utility in reducing animal testing.

The preservation of phenotype and genotype, displayed by PDX models (11), is vital to the development of new antineoplastics, not least in the age of targeted therapeutics (4, 36). Similar to Perez-Soler and colleagues (9), tissue architecture was well maintained in our NSCLC samples. In addition, using E-cadherin (epithelial) and vimentin (mesenchymal) as markers in this study it was evident that our patients were heterogeneous for the presence of EMT, implicated in drug resistance in NSCLC (37) as well as tumor invasion metastasis and progression in a range of tumor types (38), at the time of surgery and that the pattern of E-cadherin/vimentin staining was maintained in the majority of PDX lines studied.

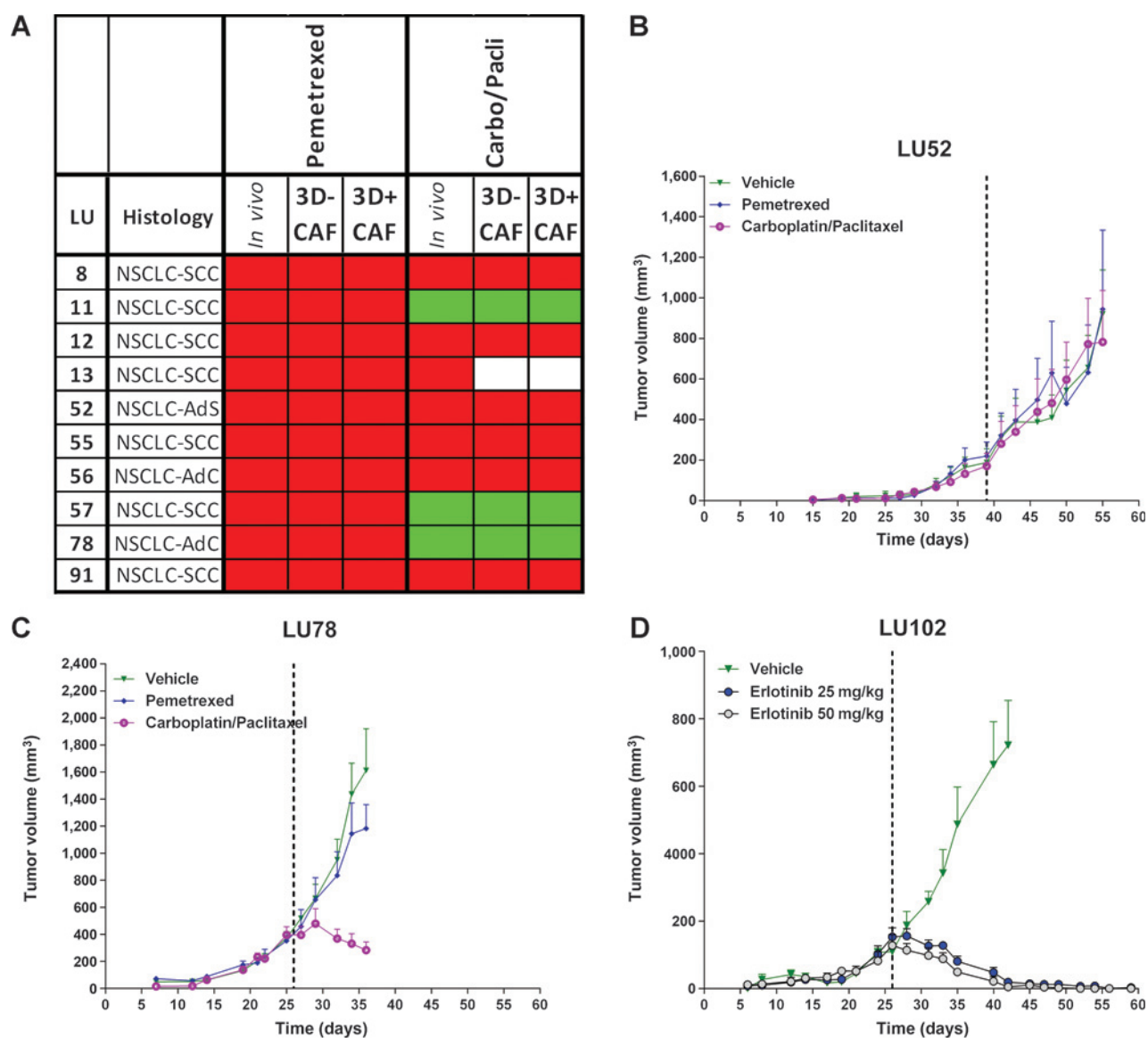


Figure 5. Comparison of *in vivo* and *ex vivo* 3D-TGA drug sensitivity of NSCLC patient lines to SOC. PDX-derived tumor cells ($n = 10$) were grown in MF-1 nude mice and treated with pemetrexed (100 mg/kg i.p. weekly), carboplatin/paclitaxel combination (50/5 mg/kg i.p. weekly), or erlotinib (25 or 50 mg/kg p.o. q.d.) or matched vehicle control. Tumor volume was determined by serial caliper measurement; error bars, 1 SD ($n > 5$ mice). A, comparison of *in vivo* and 3D-TGA data. B, example of nonresponse to SOC; LU52. C, example of response to SOC; LU78. D, response to EGFR inhibition in LU102.

The drive toward more realistic *in vitro* tumor culture has seen a great deal of effort focused on the establishment of 3D culture systems (16, 18). However, 3D models, such as spheroid assays, can be difficult to adapt to high-throughput applications, lack an ECM and are also extremely varied in their applicability to different cell types, especially primary cultures (39). The clonogenic assay (40) remains the only widely used *ex vivo* assay of xenograft or primary tumor material; however, such assays are, by definition, only able to measure growth and drug sensitivity of a subset of cells capable of anchorage-independent growth. The present study aimed to generate not only a close-to-patient system, but one that was scalable and widely applicable across different lines and tumor types.

The 3D-TGA model proved to be very adept at growing cells freshly isolated from xenograft tumors, including cells derived from a range of solid malignancies (esophageal, pancreatic, colorectal cancer, and colorectal metastases). Almost all the cells used survive and proliferate, so subsequent pharmacological assays measure effects on the entire heterogeneous population rather than a subset, providing more patient-reflective results. The assay was scalable and easily adapted to 384-well plate format. From one xenografted tumor 20+ drugs or combinations could be tested in serial dilution in either the presence or absence of CAFs/MSCs. The assay makes a step forward in the alignment to the TME by utilizing a tumor-derived matrix providing representative biochemical and

biophysical properties, including acidic pH, physiologic glucose level as well as tissue-aligned stiffness. In order to take this further, the assay incorporated the most predominant non-tumor cell type in many solid malignancies: CAFs. Patient-derived CAFs when screened in 3D coculture broadly increase proliferation of standard cell lines, and we and others also observed a similar trend with bone marrow-derived MSCs, which are one of the putative origins of cancer-associated stem cells (41). CAFs have been implicated in growth promotion, EMT, metastasis, and drug resistance, not least in the era of TKIs (32, 42) and thus their incorporation into the assay seems the first logical step in constructing multicell type *ex vivo* assays.

To date, PDX lines have been used to screen agents in standard murine xenograft assays. Due to greater heterogeneity of the tissue (in comparison with standard cell lines), higher N numbers are often required, making them expensive, time-consuming, and requiring the sacrifice of more animals. We utilized PDX lines at low passage, during the normal expansion phase for standard xenograft testing (4); the low cell number required and short time scale means that a much greater number of agents, concentrations, and combinations can be tested at early passage. Where available, we have correlated the response measured in the 3D-TGA to subsequent xenograft drug efficacy testing. In many cases, tumors were nonresponsive to SOC agents in both settings; however, LU11, LU57, and LU58 showed sensitivity to the combination of carboplatin and paclitaxel in both 3D and *in vivo* assays. In addition, patient LU102, who had an activating EGFR TK mutation, showed hypersensitivity to gefitinib and erlotinib in the 3D assay and excellent response *in vivo* (Figs. 2 and 5). Clearly the 3D-TGA does not fully recapitulate the complexity of the TME and currently cannot be used for some drugs, such as VEGF inhibitors, which act through angiogenesis not present in the 3D-TGA. However, for many other classes of drug, this assay has the potential to limit the need for further downstream xenograft testing or indeed focus that testing, minimizing both the animals used and financial costs.

It was striking that, in this study, even those in the early stage of disease had very poor response to SOC agents, suggesting that current SOC agents are badly suited to treating NSCLC and the resistance seen when used in later-stage disease may not be due *per se* to an acquired resistant phenotype (43). Of the single agents tested, carboplatin was the most efficacious with 43% responding; however, when tested in the presence of CAFs this fell to 17%. Indeed, the majority of agents were very poorly effective in the presence of CAFs both in terms of the number of patients responding and the mean IC_{50} values (Fig. 3 and Supplementary Fig. S6, respectively). The most efficacious treatment combination was gemcitabine/cisplatin when tested in the absence of CAFs, closely followed by vinorelbine/cisplatin. While the gemcitabine/cisplatin combination was much less efficacious when stromal cells were present, the combination of vinorelbine and cisplatin was almost unaffected both in the numbers of patients responding and mean IC_{50} values (Fig. 3).

There are a number of examples of fibroblasts influencing sensitivity to antineoplastics (44), and it has been seen that their secretion of a wide range of growth factors can lead to resistance to targeted therapies (32). For example, HGF secretion by fibroblasts is a key pathway mediating resistance to EGF-R, RAF, and Her-2 inhibitors (31, 32, 45). Here, we observed that in the single patient responsive to erlotinib and gefitinib, this sensitivity was dramatically reduced when cocultured with CAFs or MSCs (Fig. 2),

probably due to HGF secretion (both CAFs and MSCs were shown to have high HGF expression; data Supplementary Fig. S5). Resistance to platinum-based chemotherapies has been linked to expression of drug transporters, such as the ATP-binding cassette transporter (ABC) family; here, it was clear that stromal cells also influence drug sensitivity to platinum agents and their combinations. While the mechanism has yet to be determined, it has been recently reported that MSCs stimulate resistance to carboplatin and cisplatin via secretion of platinum-induced polyunsaturated fatty acids (46).

We observed notable individual de-sensitization to gemcitabine in the presence of CAFs (Fig. 2), and overall 10 times fewer patients were sensitive to gemcitabine in the presence of CAFs (3%) than in their absence (33%). In pancreatic cancer, a direct role for fibroblasts in gemcitabine resistance via decreased expression of caspase and its inducer STAT-1 has been demonstrated; interestingly this could be overcome by treatment with HDAC inhibitors, relieving the STAT-1 blockade and recapitulating sensitivity (47). In our study, the majority of tumors were sensitive to the HDAC inhibitor JNJ-26481585 and so, as expected, the combination with gemcitabine was also very efficacious, with specific examples of synergy between the two drugs (e.g., LU126; Fig. 4).

HDAC inhibitors have shown potent preclinical antitumor activity, but so far only two agents, vorinostat and romidepsin, have become FDA licensed with short half-lives and toxicity at higher doses being limiting factors (48). A phase I clinical trial showed JNJ-26481585 to have a much greater plasma half-life of 8.8 hours in patients with advanced solid tumors compared to other HDAC inhibitors, such as vorinostat and romidepsin (49, 50), and it shows promise for use in solid tumors either as a single agent or in combination with SOC (35). The dismal plight of those with advanced NSCLC and the observation here that even early-stage tumors are insensitive to current SOC highlights the need for novel therapeutic or combinatorial options in this setting. In the current study, 80% or greater models showed sensitivity to JNJ-26481585 and panobinostat; while the presence of CAFs increased IC_{50} s for both agents their potency meant that IC_{50} s were still in the nanomolar range. Taken together, the study provides evidence from novel, close-to-patient models that JNJ-26481585 may be of utility in the treatment of NSCLC either as a single agent or as combination therapy.

In the preclinical arena, the 3D-TGA has the potential to accelerate research utilizing PDX models by providing a rapid and scalable *ex vivo* drug-sensitivity screen of multiple single and combinatorial agents. It has also shown its utility for identifying those treatment modalities susceptible to stromal resistance. In the future, through patient-specific profiling, it may be used to direct treatment options and for biomarker identification of patient responder/nonresponder. The utility of 3D-TGAs for personalized medicine may be strengthened if the xenografting stage could be bypassed via direct embedding of disaggregated patient tumor cells into the assay, eliminating animal usage, and reducing cost and *in vitro* manipulation. A direct TME-aligned *ex vivo* 3D culture system is the subject of our future research.

Disclosure of Potential Conflicts of Interest

R. Kumari has ownership interest (including patents) in Crown Bioscience UK LTD. B.M. Hall was head of translational medicine (from 2014 to 2015) at

Medimmune. No potential conflicts of interest were disclosed by the other authors.

Authors' Contributions

Conception and design: D. Onion, R.H. Argent, S.L. Parsons, D.N. Lobo, J.C. Atherton, R. Kumari, B.M. Hall

Development of methodology: D. Onion, R.H. Argent, A.M. Reece-Smith, R.G. Pineda, S.L. Parsons, P. King, B.M. Hall

Acquisition of data (provided animals, acquired and managed patients, provided facilities, etc.): D. Onion, R.H. Argent, A.M. Reece-Smith, R.G. Pineda, P.A. Clarke, H.L. Ratan, J.P. Duffy, A.J. McKenzie, R. Kumari

Analysis and interpretation of data (e.g., statistical analysis, biostatistics, computational analysis): D. Onion, R.H. Argent, A.M. Reece-Smith, R.G. Pineda, J.C. Atherton, R. Kumari, B.M. Hall, A.M. Grabowska

Writing, review, and/or revision of the manuscript: D. Onion, R.H. Argent, A.M. Reece-Smith, S.L. Parsons, D.N. Lobo, J.P. Duffy, J.C. Atherton, R. Kumari, P. King, B.M. Hall, A.M. Grabowska

Administrative, technical, or material support (i.e., reporting or organizing data, constructing databases): M.L. Craze, R.G. Pineda

Study supervision: R.H. Argent, A.J. McKenzie, R. Kumari, A.M. Grabowska

References

- DiMasi JA, Feldman L, Seckler A, Wilson A. Trends in risks associated with new drug development: success rates for investigational drugs. *Clin Pharmacol Ther* 2010;87:272–7.
- Hutchinson L, Kirk R. High drug attrition rates—where are we going wrong? *Nat Rev Clin Oncol* 2011;8:189–90.
- Rubin EH, Gilliland DG. Drug development and clinical trials—the path to an approved cancer drug. *Nat Rev Clin Oncol* 2012;9:215–22.
- Rubio-Viqueira B, Hidalgo M. Direct in vivo xenograft tumor model for predicting chemotherapeutic drug response in cancer patients. *Clin Pharmacol Ther* 2009;85:217–21.
- Johnson JL, Decker S, Zaharevitz D, Rubinstein LV, Venditti JM, Schepartz S, et al. Relationships between drug activity in NCI preclinical in vitro and in vivo models and early clinical trials. *Br J Cancer* 2001;84:1424–31.
- Hausser HJ, Brenner RE. Phenotypic instability of Saos-2 cells in long-term culture. *Biochem Biophys Res Commun* 2005;333:216–22.
- Gillet JP, Calcagno AM, Varma S, Marino M, Green LJ, Vora MI, et al. Redefining the relevance of established cancer cell lines to the study of mechanisms of clinical anti-cancer drug resistance. *Proc Natl Acad Sci U S A* 2011;108:18708–13.
- Rubio-Viqueira B, Jimeno A, Cusatis G, Zhang X, Iacobuzio-Donahue C, Karikari C, et al. An in vivo platform for translational drug development in pancreatic cancer. *Clin Cancer Res* 2006;12:4652–61.
- Perez-Soler R, Kemp B, Wu QP, Mao L, Gomez J, Zeleniuch-Jacquotte A, et al. Response and determinants of sensitivity to paclitaxel in human non-small cell lung cancer tumors heterotransplanted in nude mice. *Clin Cancer Res* 2000;6:4932–8.
- Bankert RB, Egilmez NK, Hess SD. Human-SCID mouse chimeric models for the evaluation of anti-cancer therapies. *Trends Immunol* 2001;22:386–93.
- Chou J, Fitzgibbon MP, Mortales CL, Towler AM, Upton MP, Yeung RS, et al. Phenotypic and transcriptional fidelity of patient-derived colon cancer xenografts in immune-deficient mice. *PLoS One* 2013;8:e79874.
- Fiebig HH, Maier A, Burger AM. Clonogenic assay with established human tumour xenografts: correlation of in vitro to in vivo activity as a basis for anticancer drug discovery. *Eur J Cancer* 2004;40:802–20.
- Quail DF, Joyce JA. Microenvironmental regulation of tumor progression and metastasis. *Nat Med* 2013;19:1423–37.
- Joyce JA, Pollard JW. Microenvironmental regulation of metastasis. *Nat Rev Cancer* 2009;9:239–52.
- McMillin DW, Delmore J, Weisberg E, Negri JM, Geer DC, Klippel S, et al. Tumor cell-specific bioluminescence platform to identify stroma-induced changes to anticancer drug activity. *Nat Med* 2010;16:483–9.
- Jacks T, Weinberg RA. Taking the study of cancer cell survival to a new dimension. *Cell* 2002;111:923–5.
- Cheung KJ, Ewald AJ. Illuminating breast cancer invasion: diverse roles for cell-cell interactions. *Current Opin Cell Biol* 2014;30C:99–111.
- Cukierman E, Pankov R, Stevens DR, Yamada KM. Taking cell-matrix adhesions to the third dimension. *Science* 2001;294:1708–12.
- Friedl P, Brocker EB. The biology of cell locomotion within three-dimensional extracellular matrix. *Cell Mol Life Sci* 2000;57:41–64.
- Roskelley CD, Bissell MJ. Dynamic reciprocity revisited: a continuous, bidirectional flow of information between cells and the extracellular matrix regulates mammary epithelial cell function. *Biochem Cell Biol* 1995;73:391–7.
- Wang F, Weaver VM, Petersen OW, Larabell CA, Dedhar S, Briand P, et al. Reciprocal interactions between beta1-integrin and epidermal growth factor receptor in three-dimensional basement membrane breast cultures: a different perspective in epithelial biology. *Proc Natl Acad Sci U S A* 1998;95:14821–6.
- Debnath J, Mills KR, Collins NL, Reginato MJ, Muthuswamy SK, Brugge JS. The role of apoptosis in creating and maintaining luminal space within normal and oncogene-expressing mammary acini. *Cell* 2002;111:29–40.
- Weaver VM, Lelievre S, Lakin JN, Chrenek MA, Jones JC, Giancotti F, et al. beta4 integrin-dependent formation of polarized three-dimensional architecture confers resistance to apoptosis in normal and malignant mammary epithelium. *Cancer Cell* 2002;2:205–16.
- Frisch SM, Screaton RA. Anoiikis mechanisms. *Curr Opin Cell Biol* 2001;13:555–62.
- Krausz E, de Hoogt R, Gustin E, Cornelissen F, Grand-Perret T, Janssen L, et al. Translation of a tumor microenvironment mimicking 3D tumor growth co-culture assay platform to high-content screening. *J Biomol Screen* 2013;18:54–66.
- Sasser AK, Mundy BL, Smith KM, Studebaker AW, Axel AE, Haidet AM, et al. Human bone marrow stromal cells enhance breast cancer cell growth rates in a cell line-dependent manner when evaluated in 3D tumor environments. *Cancer Lett* 2007;254:255–64.
- Kleinman HK, Martin GR. Matrigel: basement membrane matrix with biological activity. *Semin Cancer Biol* 2005;15:378–86.
- Chou TC, Talalay P. Quantitative analysis of dose-effect relationships: the combined effects of multiple drugs or enzyme inhibitors. *Adv Enzyme Regul* 1984;22:27–55.
- Sardari Nia P, Colpaert C, Blyweert B, Kui B, Vermeulen P, Ferguson M, et al. Prognostic value of nonangiogenic and angiogenic growth patterns in non-small-cell lung cancer. *Br J Cancer* 2004;91:1293–300.
- Sardari Nia P, Colpaert C, Vermeulen P, Weyler J, Pezzella F, Van Schil P, et al. Different growth patterns of non-small cell lung cancer represent distinct biologic subtypes. *Ann Thorac Surg* 2008;85:395–405.
- Wang W, Li Q, Yamada T, Matsumoto K, Matsumoto I, Oda M, et al. Crosstalk to stromal fibroblasts induces resistance of lung cancer to epidermal growth factor receptor tyrosine kinase inhibitors. *Clin Cancer Res* 2009;15:6630–8.

Acknowledgments

This article is dedicated to the memory of Professor Sue Watson, who initiated this work and who sadly lost her battle with cancer before it was finished. The authors thank the patients who donated material to this project, and the clinical teams that made this possible. They also thank Marian Meakin and Alison Ritchie for their technical support, the research nurses and technical team of the Ex Vivo Cancer Pharmacology Centre of Excellence and to Kate Shepherd for assistance in collecting and banking material.

Grant Support

This work was funded by Janssen Research & Development, LLC and NC3RS project grant G0900765/1 both to A.M. Grabowska. Janssen Research & Development, LLC also provided a formal review of this manuscript.

The costs of publication of this article were defrayed in part by the payment of page charges. This article must therefore be hereby marked *advertisement* in accordance with 18 U.S.C. Section 1734 solely to indicate this fact.

Received July 17, 2015; revised October 30, 2015; accepted November 10, 2015; published OnlineFirst February 12, 2016.

32. Wilson TR, Fridlyand J, Yan Y, Penuel E, Burton L, Chan E, et al. Widespread potential for growth-factor-driven resistance to anticancer kinase inhibitors. *Nature* 2012;487:505–9.
33. Anne M, Sammartino D, Barginear MF, Budman D. Profile of panobinostat and its potential for treatment in solid tumors: an update. *Onco Targets Ther* 2013;6:1613–24.
34. Arts J, King P, Marien A, Floren W, Belien A, Janssen L, et al. JNJ-26481585, a novel "second-generation" oral histone deacetylase inhibitor, shows broad-spectrum preclinical antitumoral activity. *Clin Cancer Res* 2009;15:6841–51.
35. Venugopal B, Baird R, Kristeleit RS, Plummer R, Cowan R, Stewart A, et al. A phase I study of quisinostat (JNJ-26481585), an oral hydroxamate histone deacetylase inhibitor with evidence of target modulation and antitumor activity, in patients with advanced solid tumors. *Clin Cancer Res* 2013;19:4262–72.
36. Tentler JJ, Tan AC, Weekes CD, Jimeno A, Leong S, Pitts TM, et al. Patient-derived tumour xenografts as models for oncology drug development. *Nat Rev Clin Oncol* 2012;9:338–50.
37. Yauch RL, Januario T, Eberhard DA, Cavet G, Zhu W, Fu L, et al. Epithelial versus mesenchymal phenotype determines in vitro sensitivity and predicts clinical activity of erlotinib in lung cancer patients. *Clin Cancer Res* 2005;11:8686–98.
38. Polyak K, Weinberg RA. Transitions between epithelial and mesenchymal states: acquisition of malignant and stem cell traits. *Nat Rev Cancer* 2009;9:265–73.
39. Herrmann D, Conway JR, Vennin C, Magenau A, Hughes WE, Morton JP, et al. Three-dimensional cancer models mimic cell-matrix interactions in the tumour microenvironment. *Carcinogenesis* 2014;35:1671–79.
40. Hamburger AW, Salmon SE. Primary bioassay of human tumor stem cells. *Science* 1977;197:461–3.
41. Mishra PJ, Glod JW, Banerjee D. Mesenchymal stem cells: flip side of the coin. *Cancer Res* 2009;69:1255–8.
42. Cirri P, Chiarugi P. Cancer-associated-fibroblasts and tumour cells: a diabolic liaison driving cancer progression. *Cancer Metastasis Rev* 2012;31:195–208.
43. Ettinger DS, Akerley W, Bepler G, Blum MG, Chang A, Cheney RT, et al. Non-small cell lung cancer. *J Natl Compr Canc Netw* 2010;8:740–801.
44. Junttila MR, de Sauvage FJ. Influence of tumour micro-environment heterogeneity on therapeutic response. *Nature* 2013;501:346–54.
45. Straussman R, Morikawa T, Shee K, Barzily-Rokni M, Qian ZR, Du J, et al. Tumour micro-environment elicits innate resistance to RAF inhibitors through HGF secretion. *Nature* 2012;487:500–4.
46. Roodhart JM, Daenen LG, Stigter EC, Prins HJ, Gerrits J, Houthuijzen JM, et al. Mesenchymal stem cells induce resistance to chemotherapy through the release of platinum-induced fatty acids. *Cancer Cell* 2011;20:370–83.
47. Muerkoster SS, Werbing V, Koch D, Sipos B, Ammerpohl O, Kalthoff H, et al. Role of myofibroblasts in innate chemoresistance of pancreatic carcinoma—epigenetic downregulation of caspases. *Int J Cancer* 2008;123:1751–60.
48. Bose P, Dai Y, Grant S. Histone deacetylase inhibitor (HDACI) mechanisms of action: emerging insights. *Pharmacol Ther* 2014;143:323–36.
49. Grant C, Rahman F, Piekarz R, Peer C, Frye R, Robey RW, et al. Romidepsin: a new therapy for cutaneous T-cell lymphoma and a potential therapy for solid tumors. *Expert Rev Anticancer Ther* 2010;10:997–1008.
50. Kelly WK, O'Connor OA, Krug LM, Chiao JH, Heaney M, Curley T, et al. Phase I study of an oral histone deacetylase inhibitor, suberoylanilide hydroxamic acid, in patients with advanced cancer. *J Clin Oncol* 2005;23:3923–31.